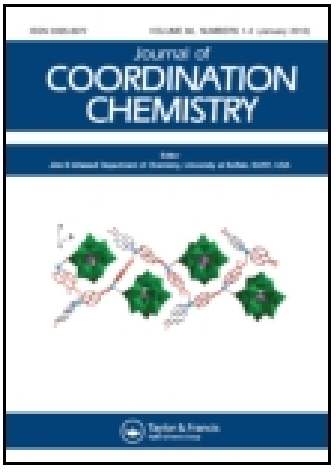

Journal of Coordination Chemistry
Publication details, including instructions for authors and subscription information:
http://www.tandfonline.com/loi/gcoo20

X-ray crystal structure of a Cu(II) complex with the antiparasitic drug tinidazole, interaction with calf thymus DNA and evidence for antibacterial activity

Ramesh Chandra Santra[a], Kushal Sengupta[a], Rajdip Dey[a], Tahsina Shireen[b], Piyal Das[a], Partha Sarathi Guin[a], Kasturi Mukhopadhyay[b] & Saurabh Das[a]

[a] Department of Chemistry (Inorganic Section), Jadavpur University, Kolkata, India

[b] School of Environmental Sciences, Jawaharlal Nehru University, New Delhi, India

Accepted author version posted online: 10 Jan 2014.Published online: 18 Feb 2014.

To cite this article: Ramesh Chandra Santra, Kushal Sengupta, Rajdip Dey, Tahsina Shireen, Piyal Das, Partha Sarathi Guin, Kasturi Mukhopadhyay & Saurabh Das (2014) X-ray crystal structure of a Cu(II) complex with the antiparasitic drug tinidazole, interaction with calf thymus DNA and evidence for antibacterial activity, Journal of Coordination Chemistry, 67:2, 265-285, DOI: 10.1080/00958972.2013.879647

To link to this article: http://dx.doi.org/10.1080/00958972.2013.879647

Journal of Coordination Chemistry, 2014
Vol. 67, No. 2, 265–285, http://dx.doi.org/10.1080/00958972.2013.879647

X-ray crystal structure of a Cu(II) complex with the antiparasitic drug tinidazole, interaction with calf thymus DNA and evidence for antibacterial activity

RAMESH CHANDRA SANTRA†, KUSHAL SENGUPTA†, RAJDIP DEY†, TAHSINA SHIREEN‡, PIYAL DAS†, PARTHA SARATHI GUIN†, KASTURI MUKHOPADHYAY‡ and SAURABH DAS*†

†Department of Chemistry (Inorganic Section), Jadavpur University, Kolkata, India
‡School of Environmental Sciences, Jawaharlal Nehru University, New Delhi, India

(*Received 7 June 2013; accepted 21 November 2013*)

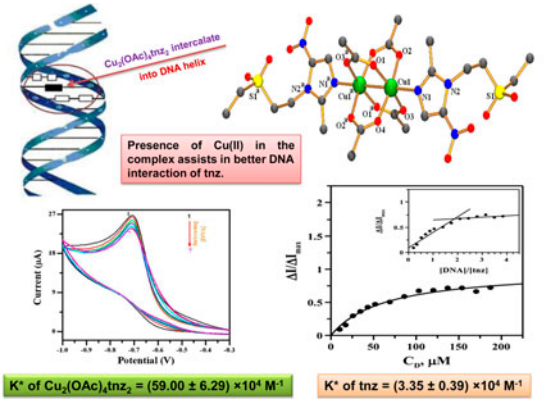

Tinidazole, a 5-nitroimidazole is active on protozoan and bacterial infections. This study made an attempt to see if a Cu(II) complex of tinidazole had comparable efficacy on chosen bacteria and fungi. The prepared complex was characterized by XRD, spectroscopy, elemental analysis cyclic voltammetry. DNA interaction was studied using cyclic voltammetry and fitted by non-linear analysis.

Interaction of metal ions with biologically active molecules like 5-nitroimidazoles modulates their electronic environment and therefore influences their biological function. In the present work, an antiparasitic drug tinidazole (tnz) was selected and a Cu(II) complex of tnz $[Cu_2(OAc)_4(tnz)_2]$ was prepared. A dinuclear paddle-wheel $[Cu_2(OAc)_4(tnz)_2]$ was obtained by single-crystal XRD and further characterized by spectroscopic techniques and cyclic voltammetry. To understand the biological implications of complex formation, interaction of tnz and its complex was studied with calf thymus DNA, bacterial and fungal cell lines. Results of calf thymus DNA interaction using cyclic voltammetry indicate the overall binding constant (K^*) of $Cu_2(OAc)_4(tnz)_2$ $[(59 \pm 6) \times 10^4\ M^{-1}]$ is

*Corresponding author. Email: sdas@chemistry.jdvu.ac.in
Kushal Sengupta was a postgraduate project student with Saurabh Das for a major part of this work.
Ramesh Chandra Santra and Kushal Sengupta have equal contribution towards the work performed.

~17 times greater than that of tnz [$(3.3 \pm 0.4) \times 10^4\ M^{-1}$]. Minimum inhibitory concentration values suggest that [$Cu_2(OAc)_4(tnz)_2$] possesses better antibacterial activity than tnz on both bacterial strains, while the activity on a fungal strain was comparable.

Keywords: X-ray diffraction; Cyclic voltammetry; Calf thymus DNA; Binding constant; MIC

1. Introduction

Binding of metal ions help to regulate and control biological functions [1–4]. Conformations of several biologically active molecules change upon complex formation with metal ions that help to improve their function. 5-Nitroimidazoles and their derivatives are of considerable interest owing to interesting chemical and pharmacological properties [5–13]. The compounds are broad spectrum antibiotics with potential toward control and cure of diseases like amoebiasis, giardiasis, human trichomoniasis, bacterial meningitis/vaginosis, and other closely related infections [7, 14–17]. However, a major drawback of these molecules is that on prolonged use they tend to be neurotoxic, established with animal model studies and also understood from post-application reports of patients administered with these drugs [18, 19]. Tinidazole (tnz) [1-(2-ethyl-sulfonyl-ethyl)-2-methyl-5-nitroimidazole] belonging to this class is an effective drug [14–17, 20] used in the treatment of protozoan and bacterial infections [5]. Compared to metronidazole (mnz), the first generation 5-nitroimidazole, some reports suggest that tnz has less toxic side effects although others differ [21–23]. Pharmacological actions of mnz and tnz are comparable but in some cases, like in giardiasis, tnz is better [22].

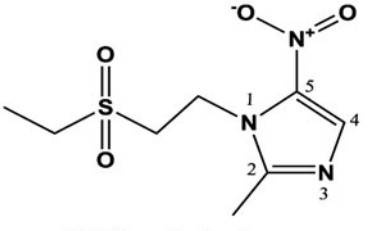

Tinidazole (tnz)

In spite of 5-nitroimidazoles showing efficacy in treating different infections, the pronounced toxic side effects [18, 19, 24] are a hindrance to their use. Lack of suitable alternatives that match their efficacy still allow them to be used [25, 26]. Since 5-nitroimidazoles are so important for several infections, suitable structural modifications that do not affect drug efficacy but are able to minimize the formation of radicals responsible for toxic side effects would be important. Coordinating 5-nitroimidazoles to metal ions could be one such alternative since their introduction would affect the electronic environment of the drug [1–4]. The result could be that formation of radicals and/or anions by 5-nitroimidazoles responsible for toxic side effects could either be stopped or controlled. Since these same radicals or ions are involved in drug action, such modifications could also affect the beneficial aspects of these molecules, i.e. cytotoxic actions could get jeopardized. Nevertheless, complex formation offers an opportunity to explore how they compare with 5-nitroimidazoles.

A very recent study on 5-nitroimidazoles shows that these drugs bind to proteins involved in the thioredoxin-mediated redox network and disrupt the redox equilibrium inhibiting

thioredoxin reductase and depleting intracellular thiol pools in micro-aerophilic parasites, *Entamoeba histolytica*, *Trichomonas vaginalis*, and the human parasite *Giardia lamblia* [27]. Several such molecules act as effective drugs by targeting the DNA of the target organism [2, 10, 28]. In our case, we examine if a metal complex of tnz is a better binder of DNA than tnz [28]. Although reports on DNA interaction of 5-nitroimidazoles exist [29, 30], work on their metal complexes is scarce. However, some recent reports show copper complexes of other ligands interact with DNA or proteins [28, 31–33], which is why there is a constant effort to prepare Cu(II) complexes [34]. In our case, the purpose behind pursuing a DNA interaction study for tnz and its Cu(II) complex was to see if the possibility for a decrease in cytotoxic action upon complex formation owing to decreased nitro radical anion generation was suitably compensated by increased DNA interaction that could eventually make the complexed form of tnz better [28].

2. Experimental setup

2.1. *Materials*

Tnz was purchased from Sigma–Aldrich, USA. The compound was dissolved in hot methanol and crystalline forms were obtained by slow evaporation of the solvent, isolated by filtration. Copper(II) acetate [$Cu(OAc)_2 \cdot H_2O$] was obtained from E. Merck, India. Calf thymus DNA was purchased from Sisco Research Laboratories, India, and dissolved in phosphate buffer (pH ~7.4) containing 120 mM NaCl (AR grade, Merck, Germany). The purity of DNA was checked from the absorbance ratio A_{260}/A_{280}. The value being in the range $1.8 < A_{260}/A_{280} < 1.9$ suggested no further de-proteinization was required. The concentration of calf thymus DNA in terms of nucleotide was determined by taking $\varepsilon_{260} = 6600\ M^{-1}\ dm^3\ cm^{-1}$. The quality of calf thymus DNA was also verified from the characteristic CD band at 260 nm. Physiological condition (pH ~7.4) was maintained using phosphate buffer that contained 120 mM NaCl, 3.5 mM KCl, 1 mM $CaCl_2$, and 0.5 mM $MgCl_2$. Reagents required for preparation of the buffer were obtained from E. Merck, India. NaCl ($0.500\ M\ dm^{-3}$) (AR grade, Merck, Germany) was used to maintain ionic strength. For cyclic voltammetric experiments, tetrabutyl ammonium bromide (AR grade) from Spectrochem (India) Pvt. Ltd. was used as supporting electrolyte in non-aqueous medium, while KCl (E. Merck, India) was used as supporting electrolyte in aqueous medium. Stock solutions of tnz and $[Cu_2(OAc)_4(tnz)_2]$ ($10^{-4}\ M\ dm^{-3}$) were prepared by weighing exact amounts. Subsequently, solutions were diluted for use. All solutions were prepared in triple distilled water.

Bacterial and fungal strains: *Staphylococcus aureus* (ATCC 29213), *Escherichia coli* (ATCC 25922), and *Candida albicans* (CAF 2-1) were used in this study [35–37]. These strains were stored at −70 °C in 15% (vol/vol) glycerol until subcultured onto respective media. Bovine heart infusion media were used for culturing bacterial cells, whereas yeast extract-peptone-dextrose media were used for culturing fungal cells. Both media were purchased from High Media Laboratories, India.

2.2. *Methods*

2.2.1. Preparation of $[Cu_2(OAc)_4(tnz)_2]$. The complex of tnz, $[Cu_2(OAc)_4(tnz)_2]$, was prepared according to the methods described for mnz [38, 39]. Tnz (0.494 g, 2.00 mM) was

added to a solution of $Cu(OAc)_2 \cdot H_2O$ (0.399 g, 2.00 mM) in hot methanol (25 mL). The mixture was heated under reflux at ~50 °C for 8 h. After a week, a green crystalline compound was obtained by slow evaporation of the solvent which was filtered and recrystallized.

Yield: 70%. Anal. Calcd (%) for $[Cu_2(OAc)_4(tnz)_2]$, i.e. $C_{24}H_{38}N_6O_{16}S_2Cu_2$: C, 33.58; H, 4.43; N, 9.80. Found: C, 33.31; H, 4.44; N, 9.89. Cu(II) present in the complex was estimated using a standard procedure [40] and the result obtained was 14.66% (Anal. Calcd 14.80%).

2.2.2. Crystallographic data collection and refinement. A suitable green single crystal of $[Cu_2(OAc)_4(tnz)_2]$ was mounted on a thin glass fiber with the help of commercially available super glue. X-ray single-crystal data collection was done at room temperature (298 K) using a Bruker APEX II diffractometer, equipped with a normal focus, sealed tube X-ray source with graphite-monochromated Mo-Kα radiation ($\lambda = 0.71073$ Å). The data were integrated using SAINT [41] and absorption corrections were made with SADABS. Structures were solved by SHELXS 97 [42, 43] using the Patterson method followed by successive Fourier and difference Fourier synthesis. Full-matrix least-squares refinements were performed on F^2 using SHELXL 97 [42, 43] with anisotropic displacement parameters for all non-hydrogen atoms. During refinement of the complex, all calculations were carried out using SHELXL 97, SHELXS 97, PLATON v1.15 [44], ORTEP-3v2 [45], and WinGX system Ver-1.80 [46]. Data collection, structure refinement parameters, and crystallographic data for the compound are provided in table 1. Selected bond lengths and angles are given in table 2.

Table 1. Crystallographic and structural refinement parameters for $[Cu_2(OAc)_4(tnz)_2]$.

Empirical formula	$C_{24}H_{38}N_6O_{16}S_2Cu_2$
Formula weight	857.84
Cryst. syst.	Monoclinic
Space group	$P2_1/c$
a (Å)	14.1124(9)
b (Å)	8.9616(6)
c (Å)	14.0024(9)
α (°)	90
β (°)	100.880(2)
γ (°)	90
V (Å^3)	1739.1(2)
Z	2
D_{Calcd} g cm^{-3}	1.638
μ (Mo-Kα), mm^{-1}	1.422
F (0 0 0)	884
θ range (°)	1.5–27.6
No. of reflns. collected	23428
No. of independent reflns.	4035
R_{int}	0.035
No. of reflns. $I > 2\sigma(I)$	3618
Goodness-of-fit (F^2)	1.05
R_1 ($I > 2\sigma(I)$)[a]	0.0291
wR_2[a]	0.0865
Residuals (e/Å^3)	−0.50, 0.38

[a] $R_1 = \Sigma||F_o| - |F_c||/\Sigma|F_o|$; $wR_2 = [\Sigma\,(w(F_o{}^2 - F_c{}^2)^2)/\Sigma w\,(F_o{}^2)^2]^{1/2}$.

Table 2. Selected bond lengths (Å) and angles (°) for $[Cu_2(OAc)_4(tnz)_2]$.

Bond lengths (Å)			
Cu1–O1	1.9860(15)	Cu1–O2	1.9594(15)
Cu1–O3	1.9713(16)	Cu1–O4	1.9686(15)
Cu1–N1	2.1750(16)		
Bond angles (°)			
O1–Cu1–O3	168.43(7)	O1–Cu1–O4	89.05(7)
O1–Cu1–N1	93.00(6)	O2–Cu1–O3	90.00(7)
O2–Cu1–O4	168.14(6)	O2–Cu1–N1	96.90(6)
O3–Cu1–O4	89.67(7)	O3–Cu1–N1	98.57(6)
O4–Cu1–N1	94.87(6)	Cu1–O1–C11[a]	120.08(14)
Cu1–O2–C9	124.11(13)	Cu1–O3–C11	126.20(14)
Cu1–O4–C9[a]	122.17(13)	Cu1–N1–C1	132.98(13)
Cu1–N1–C3	120.30(12)	O1–Cu1–O2	88.91(7)

Notes: Symmetry code: $a = 1 - x, 2 - y, 1 - z$.

2.2.3. Physical measurements. A CD spectropolarimeter J815, JASCO, Japan, was used to determine the quality of calf thymus DNA. UV–Vis spectra of tnz and $[Cu_2(OAc)_4(tnz)_2]$ were recorded from 200 to 800 nm on a Shimadzu UV-1700 Pharmaspec, Shimadzu, Japan. FT-IR data of solid samples in KBr pellets were recorded using a Perkin Elmer RX-I spectrophotometer. Mass spectrum was recorded on a Micromass Q-Tof micro™, Waters Corporation. Elemental analysis of the complex was carried out using a Perkin-Elmer 2400 Series-II CHN analyzer. Magnetic susceptibility measurements of powdered samples at 303 K were recorded by the Gouy method using a Magway MSB MK1, Sherwood Scientific Ltd. EPR was recorded on a JEOL JES-FA 200 ESR spectrophotometer. Fluorescence experiments were done using a fluorescence spectrophotometer (model JOBIN YVON Fluoromax 3).

2.2.4. Cyclic voltammetry of tnz and $[Cu_2(OAc)_4(tnz)_2]$. Cyclic voltammetric studies were carried out using a potentiostat/galvanostat Model 263A, Princeton Applied Research supported by EG & G software. A conventional three-electrode system was used. A glassy carbon electrode of surface area 0.1256 cm^2 served as the working electrode, a platinum wire was the counter electrode, while Ag/AgCl, satd. KCl was the reference electrode (0.199/V). Before each scan, the solution was degassed for 30 min using high-purity argon. Temperature was maintained using a circulating water bath. A pH meter (Elico Li 613, India) was used for recording pH. Results were analyzed by the Randles–Sevcik equation [equation (1)] [47, 48] followed by simulation using esp24b software [49–51];

$$i_{pc} = (2.69 \times 10^5) \cdot n^{3/2} \cdot D_0^{1/2} \cdot A \cdot C \cdot v^{1/2} \quad (1)$$

where i_{pc} refers to the current at the cathodic peak potential in amperes, n indicates total number of electrons involved in electrochemical reduction, D_0 was the diffusion coefficient of the species, A refers to area of the electrode in cm^2, C is the concentration of the substance in M cm^{-3}, and v refers to scan rate in V s^{-1}.

2.2.5. Interaction of the compounds with calf thymus DNA. Interaction of the compounds with ct DNA was not done using UV–Vis spectroscopy as the difference between λ_{max} of tnz (317 nm) and λ_{max} of ct DNA (260 nm) was less than 60 nm. This minimum difference needs to be kept in order to avoid interference between the spectrum

of the compound under study with that of DNA [28]. For the complex, the molar extinction coefficient at 713 nm was so low ($\varepsilon = 210\ M^{-1}\ cm^{-1}$) that DNA interaction could not be followed by UV–Vis spectroscopy as the chances of error for low ε values are very high. For these two reasons, we chose to follow the interaction of the compounds with ct DNA by cyclic voltammetry [28]. Reduction of the $-NO_2$ group was monitored for electrochemical activity. Results of the titration of each compound with ct DNA were analyzed by monitoring the reduction peak potential of tnz and that of the complex. The cyclic voltammetric data were analyzed by different equations considering the compound–DNA equilibrium [equation (2)] [52–55].

$$L + D = L - D \tag{2}$$

$$K_d = \frac{C_L C_D}{C_{LD}} \tag{3}$$

where C_L represents the concentration of free tnz or $[Cu_2(OAc)_4(tnz)_2]$, while C_D and C_{LD} represent the concentration of free ct DNA and the formed DNA–tnz or DNA-$[Cu_2(OAc)_4(tnz)_2]$ adducts, respectively. K_d was the dissociation constant equal to $1/K_{app}$; K_{app} indicates the apparent binding constant for each compound to ct DNA. For each compound, the cathodic peak current (I_{pc}) was linearly proportional to concentration, so that the decrease could be used to create binding isotherms. Using the linear relationship between cathodic peak current and concentration of the compounds, equations (4–6) were derived [55].

$$K_d = \frac{\left[C_0 - \left(\frac{\Delta I}{\Delta I_{max}}\right) C_0\right]\left[C_{D-} \left(\frac{\Delta I}{\Delta I_{max}}\right) C_0\right]}{\left(\frac{\Delta I}{\Delta I_{max}}\right) C_0} \tag{4}$$

$$C_0 \left(\frac{\Delta I}{\Delta I_{max}}\right)^2 - (C_0 + C_D + K_d)\left(\frac{\Delta I}{\Delta I_{max}}\right) + C_D = 0 \tag{5}$$

$$\frac{1}{\Delta I} = \frac{1}{\Delta I_{max}} + \frac{K_d}{\Delta I_{max}(C_D - C_0)} \tag{6}$$

ΔI was the change in cathodic peak current (I_{pc}) for tnz or $[Cu_2(OAc)_4(tnz)_2]$ for each point of their respective titration curves. ΔI_{max} was the same parameter that provided the maximum change in ΔI when either compound was totally bound to ct DNA. C_0 indicates initial concentration of the compounds. The double reciprocal plot [equation (6)] provided a value for ΔI_{max} as the inverse of the intercept, while the slope of the plot provided an estimate of K_d. Using ΔI_{max} from equation (6), K_d could also be evaluated using non-linear curve fit analysis [equations (4) and (5)]. Knowing values for K_d from both approaches, the apparent binding constant of the molecules to ct DNA was evaluated. Since K_{app} provided the binding constant of a molecule binding to an isolated site, in order to calculate overall binding constant (K^*), K_{app} was multiplied with the site size n; n denoting the number of nucleotide bases bound to a molecule of each compound interacting with ct DNA.

Considering the interaction of tnz and $[Cu_2(OAc)_4(tnz)_2]$ with ct DNA to be non-specific and non-cooperative, the relation between the ratio, r, of the concentration of each bound compound C_b [represented in the equilibrium, equation (1) as C_{LD}] to the total

concentration of ct DNA C_D, $r = \frac{C_b}{C_D}$, and C_f, concentration of the free compound was fitted to equation (7) [56].

$$\frac{r}{C_f} = K(1 - nr)\left[\frac{1 - nr}{(1 - (n-1)r)}\right]^{n-1} \tag{7}$$

C_f was obtained from the I_{pc} at the cathodic peak potential for each compound with "n" indicating binding site size in the nucleotide bases for each bound molecule interacting with double-stranded ct DNA. An advantage of using equation (7) over the ones described earlier was that both overall binding constant and site size of interaction could be obtained directly.

In order to establish the mode of interaction of $[Cu_2(OAc)_4(tnz)_2]$ with ct DNA, a qualitative study was performed where 195 µM ct DNA was saturated with ethidium bromide (EtBr) [taken ~20 times more] and allowed to stand for 1 h [53]. The solution was then excited at 510 nm and emission maxima measured at 610 nm. Thereafter, $[Cu_2(OAc)_4(tnz)_2]$ was added to this solution and its concentration was 47.62 µM. Immediately after addition of $[Cu_2(OAc)_4(tnz)_2]$, the solution was again excited at 510 nm and emission measured at 610 nm. Thereafter, excitation at 510 nm was done at regular intervals of 10 min for 30 min.

2.2.6. Biological assay with two bacterial and a fungal cell line. The *in vitro* antimicrobial activities of these compounds with gram-positive bacteria *S. aureus* (ATCC 29213), gram-negative bacteria *E. coli* (ATCC 25922), and the fungus *C. albicans* (CAF 2–1) were studied by performing minimum inhibitory concentration (MIC) assay. This was determined in Mueller Hinton Broth (MHB, HiMedia Laboratories, India) by a micro-dilution technique using a 96-well round-bottomed microtitre plate (Corning Incorporated, Corning, NY) according to Clinical Laboratory Standards Institute (CLSI 2006b, formerly NCCLS) guidelines with a final inoculum of 2×10^5 CFU/mL. MIC was defined as the lowest drug concentration preventing visible turbidity after 18 h of incubation at 37 °C.

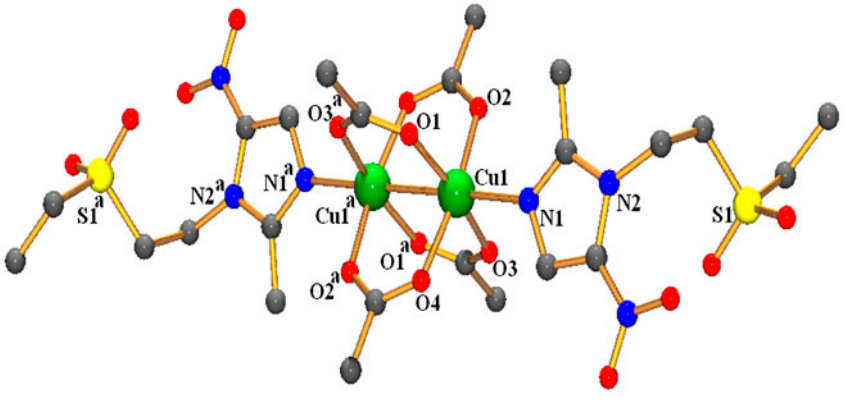

Figure 1. Atom labeling diagram of $[Cu_2(OAc)_4(tnz)_2]$.

3. Results and discussion

3.1. *Structure description of $[Cu_2(OAc)_4(tnz)_2]$*

The compound crystallizes in a monoclinic $P2_1/c$ space group. Single-crystal X-ray diffraction analysis reveals a dimeric complex of copper(II) with coppers bridged by acetates and each connected to monodentate tnz (figure 1). Each five-coordinate Cu(II) with CuO_4N chromophore shows exactly square pyramidal geometry with an Addison parameter (τ) value of 0.00 [57]. Each Cu(II) was linked to four oxygens (O1, O2, O3, and O4) of acetates in equatorial positions, bond length lying between 1.959(15) and 1.986(15) Å. The axial site was occupied by N1 of the imidazole ring of tnz with bond distance 2.175(16) Å. Other selected bond lengths and angles are reported in table 2.

In the crystal packing, two different acetates connect the Cu(II) centers to form a paddle-wheel $Cu_2(CO_2)_4$ dinuclear secondary building unit [58–61] separated by 2.625 Å representing a moderately strong Cu(II)···Cu(II) interaction. The dimers are associated through intermolecular C–H···O interaction between O8 of nitro and the methylene hydrogens (H5a and H5b) located at the side chain of the imidazole ring with C5–H5A···O8 of 2.40 Å, 150° and C5–H5B···O8 of 2.27 Å, 124°, respectively (figure 2). This C–H···O interaction is responsible for the supramolecular 3-D arrangement oriented along the *c*-axis (figure S1, see online supplemental material at http://dx.doi.org/10.1080/00958972.2013.879647).

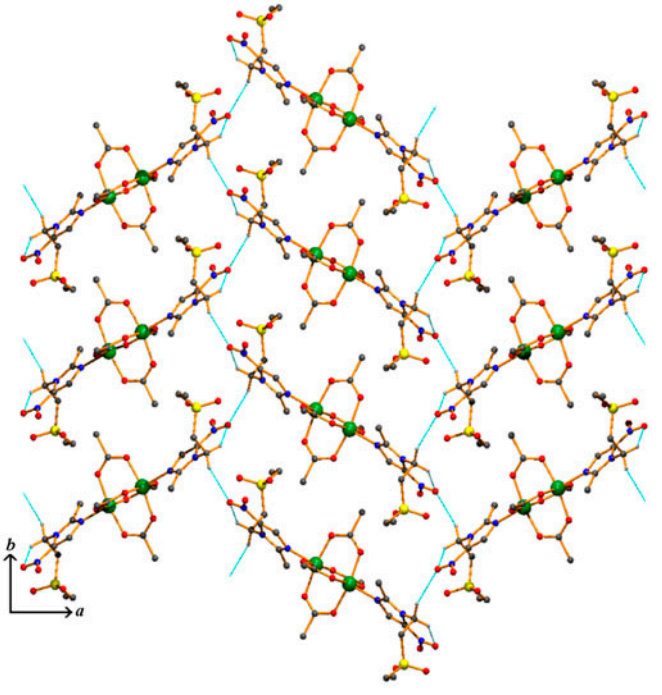

Figure 2. C–H···O interaction in $[Cu_2(OAc)_4(tnz)_2]$ (cyan line) along the *c*-axis.

3.2. *Spectroscopic studies*

3.2.1. UV–Vis spectra. Both tnz and $[Cu_2(OAc)_4(tnz)_2]$ were dissolved in pure ethanol (1×10^{-3} M) and spectra were recorded at different time intervals. No change was observed; 10 mL of the above solution was then taken and a 100 mL aqueous solution was prepared by adding 90 mL water containing Tris buffer and 120 mM NaCl. The solution thus prepared was stable and spectra were taken at different time intervals showing no change. Hence, the complex was stable in an aqueous solution containing Tris buffer and 10% ethanol. Tnz and $[Cu_2(OAc)_4(tnz)_2]$ show intense UV bands at 300–330 nm ($\varepsilon = 18540\ M^{-1}\ cm^{-1}$) with a shoulder at 235 nm. Bands in this region for the complex were very similar to that of tnz and attributed to intra-ligand (IL) transitions with some orbital overlap from Cu(II). The band at 713 nm (14,084 cm^{-1}) for the complex was assigned to the characteristic Cu(II) d–d transition (d_{xy}, $d_{yz} \rightarrow d_{x^2-y^2}$) [59] as a very weak absorption ($\varepsilon = 210\ M^{-1}\ cm^{-1}$).

3.2.2. IR spectra. The IR spectrum of tnz (figure S2) shows a band at 1522 cm^{-1} assigned to $\nu_{(C=N)}$ imidazole ring stretch which shifts to higher wave numbers (1545–1561 cm^{-1}) for the Cu(II) complex (figure S3), indicating coordination of the imidazole nitrogen (N_3) to copper. The two NO_2 stretches, $\nu_{as} = 1465\ cm^{-1}$ and $\nu_s = 1367\ cm^{-1}$, in $[Cu_2(OAc)_4(tnz)_2]$ were similar to tnz. The splitting of the NO_2 bands, $\Delta\nu(NO_2)$ ~100 cm^{-1}, in case of tnz and $[Cu_2(OAc)_4(tnz)_2]$ clearly indicates that the nitro did not participate in coordinating copper [39]. Similarly, the splitting of the SO_2 stretching vibrations, 1303 cm^{-1} (ν_{as}) and 1122 cm^{-1} (ν_s), ($\Delta\nu$ = ~180 cm^{-1}), was similar for tnz and $[Cu_2(OAc)_4(tnz)_2]$, indicating SO_2 did not take part in binding. IR spectrum of $[Cu_2(OAc)_4(tnz)_2]$ shows two intense bands at 1627 and 1428 cm^{-1}, respectively, that were not found for tnz (figure S2), characteristic of $\nu_{as}(CO_2)$ and $\nu_s(CO_2)$ and the difference between both values ($\Delta\nu(CO_2) = 199\ cm^{-1}$), generally observed for bridging acetates [39].

3.2.3. Mass spectrum of $[Cu_2(OAc)_4(tnz)_2]$. According to the crystal data, the molecular ion peak for the compound should be at $m/z = 856.6$ (^{63}Cu and ^{63}Cu) or 858.6 (^{63}Cu and ^{65}Cu) or 860.6 (^{65}Cu and ^{65}Cu). However, indications for such peaks were not prominent (figure S4). The acetate ions depart as radicals from the complex leaving behind an electron on the metal center as evidenced by the nature of the mass spectrum. When one acetate ion departs, theoretical values of m/z for the species should occur at 797.6 (^{63}Cu and ^{63}Cu) or 799.6 (^{63}Cu and ^{65}Cu) or 801.6 (^{65}Cu and ^{65}Cu). The peak at $m/z = 798.7$ along with other peaks in the vicinity (isotopic distribution) indicates formation of such species. Small peaks with $m/z = 676.63$ and 678.65 were due to species where two Cu(II) atoms, each linked to a tnz, joined to each other by one acetate bridge. Experimental peaks at $m/z = 615.79$, 617.79, 618.81, and 619.80 indicate the formation of $Cu_2(tnz)_2$ for which the theoretical m/z values were 620.6 (^{63}Cu and ^{63}Cu), 622.6 (^{63}Cu and ^{65}Cu), and 624.6 (^{65}Cu and ^{65}Cu), respectively. Difference in m/z values between those theoretically expected and experimentally found was due to loss of one or more hydrogen atoms from the structure. From $Cu_2(tnz)_2$, if one Cu departs, then the species obtained should have $m/z = 557.6$ (^{63}Cu) or 559.6 (^{65}Cu). Experimental peaks at 556.82 and 558.8 agree. Indications for Cu–tnz were obtained at 309.87 (theoretical $m/z = 310.3$ for ^{63}Cu) and 311.88 (theoretical $m/z = 312.3$ for ^{65}Cu).

3.3. *EPR spectrum and magnetic property of $[Cu_2(OAc)_4(tnz)_2]$*

The effective magnetic moment recorded at 303 K for $[Cu_2(OAc)_4(tnz)_2]$ (1.34 BM) was significantly lower than the normal value expected for d^9 configuration of Cu(II) and indicated reasonably strong antiferromagnetic coupling between the Cu(II) compounds. The value was close to μ_{eff} values reported for Cu(II) acetates and other binuclear Cu(II) compounds [39, 62] and suggests the existence of a dimeric structure with an interaction between Cu(II) centers by super exchange involving the bridging acetates. This super exchange in addition to Cu–Cu interaction is believed to play a part in the magnetic interaction resulting in subnormal magnetic moments.

The EPR spectrum at X-band frequency for powdered $[Cu_2(OAc)_4(tnz)_2]$ taken from 0 to 800 mT at 25 °C showed three signals at 28 mT(Hz_1), 460 mT ($H\perp_2$), and 600 mT (Hz_2) as expected for acetate-bridged dinuclear Cu(II) complexes (figure S5). The spin Hamiltonian for the triplet state of dimeric copper(II) compounds is given by [63],

$$H = \beta\ \mathrm{HgS} + DSz^2 + E(\mathrm{S}x^2 - \mathrm{S}y^2) - 2/3D$$

where D and E are the zero-field splitting parameters, β is the Bohr magneton, and x, y, and z are principal axes coordinate system fixed with respect to the Cu–Cu bond. However, in a powder sample, it is impossible to align the magnetic field along a given direction and the observed spectrum is the sum over all possible orientations. Three resonance fields observed for such axially symmetric complexes and the g values ($g_\parallel$ and $g_\perp$) at room temperature for a powdered sample are related by the following equations:

$$H\perp_2 = (g_e/g_\perp)^2[H_0(H_0 + D')]$$

$$Hz_1 = -(g_e/g_z)(H_0 - D')$$

$$Hz_2 = (g_e/g_z)(H_0 + D')$$

where $H_0 = h\nu/g_e\beta$ and $D' = D/g_e\beta$. The g values obtained as 2.36 ($g_\parallel$) and 2.04 ($g_\perp$) compare well with previous data [64–68].

3.4. *Cyclic voltammetric studies*

The cyclic voltammogram of tnz in methanol obtained at a scan rate of 0.1 V s^{-1} shows a reduction peak at −0.850 V against Ag/AgCl, satd. KCl ($E_{½} = -0.835$ V) [figure 3(a)]. The peak was assigned to reduction of the $–NO_2$ group [13, 69, 70] on the imidazole ring of tnz. The cyclic voltammogram of $[Cu_2(OAc)_4(tnz)_2]$ having similar concentration and scan rate shows a reduction peak at −0.890 V against Ag/AgCl, satd. KCl ($E_{½} = -0.85$ V) [figure 3(b)]. The metal-centered reduction peak of $[Cu_2(OAc)_4(tnz)_2]$ for Cu(II)/Cu(I) was obtained at 0.120 V against Ag/AgCl, satd. KCl ($E_{½} = 0.161$ V) (figure S6). Voltammograms for the reduction of the nitro group were also obtained at various scan rates for both compounds. Thus, possible chemical reactions that could accompany electrochemical processes were obtained.

For both compounds, I_{pc} was plotted against the square root of the scan rate (figure 4). Straight lines were obtained passing through the origin, clearly demonstrating the

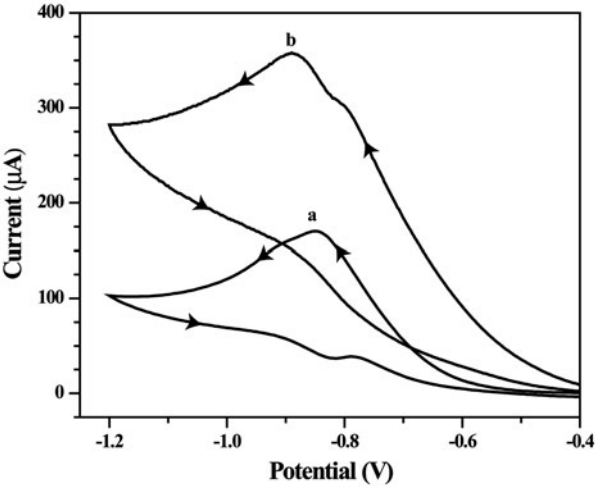

Figure 3. Cyclic voltammogram of 1 mM tnz (curve *a*) and 1 mM $[Cu_2(OAc)_4(tnz)_2]$ (curve *b*) in pure methanol, scan rate = 0.1 Vs^{-1}; $T = 25$ °C.

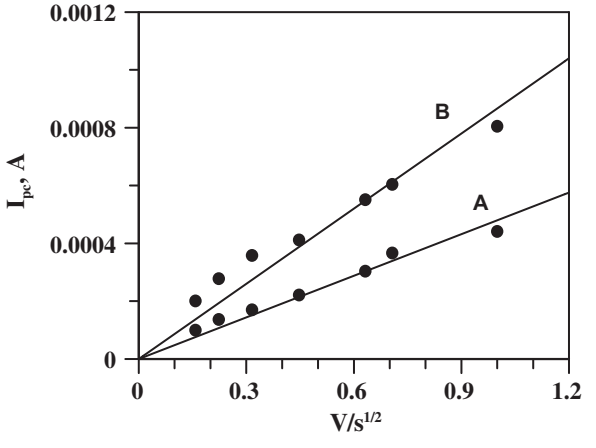

Figure 4. Dependence of cathodic peak current on square root of scan rate for the reduction of tnz (A) and $[Cu_2(OAc)_4(tnz)_2]$ (B) in pure methanol; $T = 25$ °C.

compounds undergo reduction in a diffusion-controlled pathway and that there was no adsorption on the electrode surface. Although the entire process of reduction in aqueous medium was not completely reversible, a rough estimate of the diffusion coefficient (D_0) for each compound could be obtained from figure 3 using the Randles–Sevcik equation [equation (1)] [47, 48]. For this, the number of electrons involved in reduction was taken as four. Values were 2.41×10^{-6} and 9.89×10^{-6} for tnz and $[Cu_2(OAc)_4(tnz)_2]$, respectively.

Previous studies on mnz in aqueous DMF showed that the nitro group initially undergoes a reversible one-electron reduction to a radical anion, followed by an irreversible three-electron reduction (of the nitro radical anion) to hydroxylamine derivatives [9, 13].

These studies also showed, as the percentage of DMF in aqueous DMF (solvent) decreased, that the two separate peaks gradually got closer and eventually merge to a single irreversible four-electron reduction wave. Previous workers also reported the absence of two peaks for the reduction of the $-NO_2$ group in aqueous solution (buffer, pH ~7.4) or methanol [9, 13]. The electrochemical process in such solvents is most likely a "one-electron reduction" followed by a "three-electron reduction". We made an attempt to check this by using simulations with the help of esp24b software [49–51]. Using the voltammograms obtained at different scan rates for both compounds, the simulation was carried out for a "one-electron reduction" step followed by a "three-electron reduction" as well as for one-step "four-electron reduction" [13, 69]. We found that the former approach provided a better fit to the experimental data, thus supporting a two-step process. Figure 5 shows a typical cyclic voltammogram of tnz at a scan rate of 0.1 V s^{-1} along with the simulated curve shown by a dotted line that followed scheme 1.

Incorporation of a homogenous chemical reaction in the simulation while considering interaction of the "one-electron reduction" product (T^-) with the four-electron (T^{4-}) to create new species *A* and *B* was important since considering it the fit of the simulated curve to

Electrochemical reaction in aqueous medium: $T + e = T^-$

$T^- + 3e = T^{4-}$

Homogeneous chemical reaction: $T^- + T^{4-} = A + B$ **(Products)**

Scheme 1.

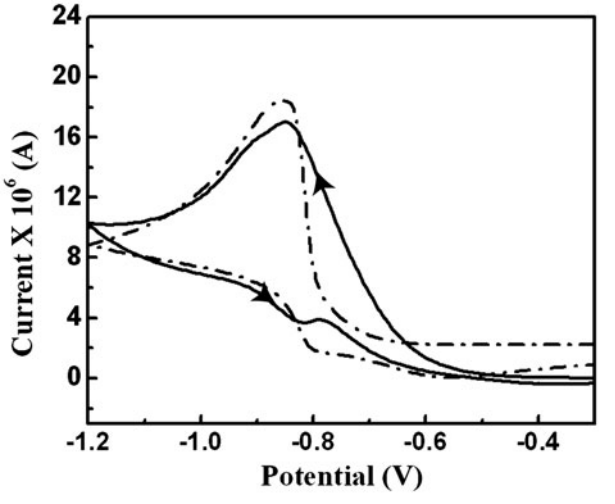

Figure 5. Cyclic voltammogram of 1000 µM tnz (——) recorded at 0.4 Vs^{-1} potential sweep rate in 0.1 M KCl as supporting electrolyte in aqueous solution (buffer, pH ~7.4) using a glassy carbon electrode at 298 K. In case of experiment and simulation 235 Ω was included. Dotted (- - - - -) line is the simulated curve for the process as represented in scheme 1. Simulation parameters: $K_{e,1} = 1.0 \times 10^{-3}$ cm s^{-1}, $\alpha_1 = 0.51$, $E_1 = -0.70$ V *vs.* Ag/AgCl saturated KCl; $K_{e,2} = 1.0 \times 10^{-2}$ cm s^{-1}, $\alpha_2 = 0.0001$, $E_2 = -0.85$ V *vs.* Ag/AgCl saturated KCl, $D_0 = 1.0 \times 10^{-4}$ cm^2 s^{-1}, 5.0×10^{-6} cm^2 s^{-1}, 1.0×10^{-5} cm^2 s^{-1}, 1.0×10^{-5} cm^2 s^{-1} and 3.0×10^{-5} cm^2 s^{-1} for *T*, T^-, T^{4-}, *A* and *B*, respectively (scheme 1). K_f and K_b for the homogenous reactions were 3000 and 10, respectively. A (surface area of the electrode) = 0.1256 cm^2. Cathodic currents were taken as positive.

the experimental improved substantially. The homogeneous chemical reaction considered during the simulation also explains why oxidation peaks were not obtained and the cyclic voltammograms were irreversible. This behavior in aqueous solution (buffer, pH ~7.4) and methanol was unlike that reported for mnz in aqueous DMF, where the "one-electron reduction" step was almost completely reversible [13]. At very high scan rates, however, there were some signs of an oxidation peak indicating that the reduced species T^{-} and T^{4-} did not get sufficient time to interact before they were oxidized in the reverse scan. This implies that at higher scan rates the electrochemical reaction outweighs the homogeneous chemical reaction by not providing sufficient time for the reduced species to interact. Hence, a variation of scan rate for both compounds, along with simulations performed on each, enabled us to understand the mechanism of the electrochemical reduction of tnz and $[Cu_2(OAc)_4(tnz)_2]$. Simulation parameters and diffusion coefficient D_0 determined through

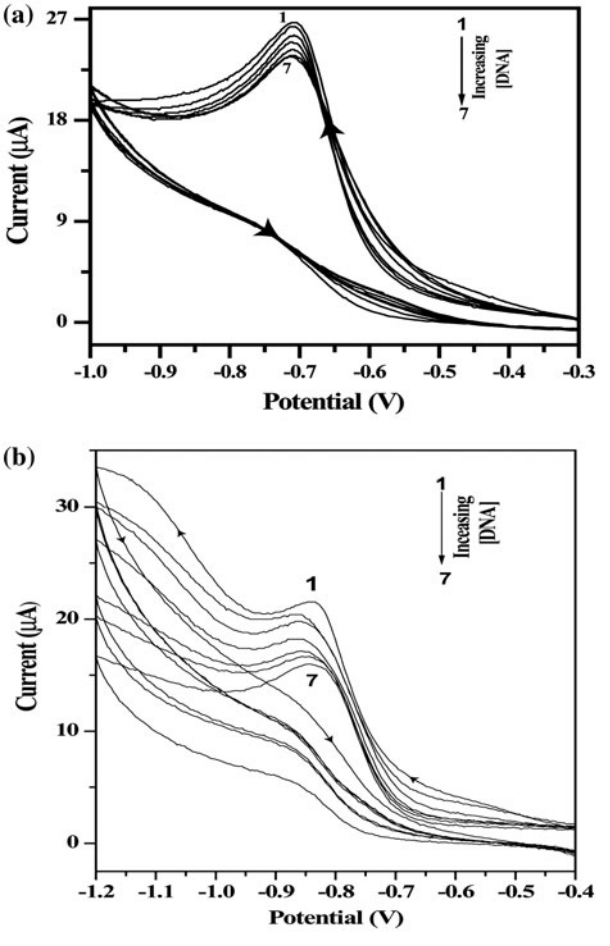

Figure 6. Cyclic voltammogram for DNA titration of (a) 50 μM tnz in absence (1) and presence of different concentrations of ct DNA: 10.48 μM (2), 26.15 μM (3), 43.48 μM (4), 86.42 μM (5), 137.25 μM (6), 170.73 μM (7) and (b) 25 μM $[Cu_2(OAc)_4(tnz)_2]$ in absence (1) and presence of different concentrations of ct DNA: 32.20 μM (2), 39.39 μM (3), 48.93 μM (4), 54.88 μM (5), 60.82 μM (6), 72.65 μM (7). For each case pH 7.4; [NaCl] = 120 mM; T = 25 °C.

simulation for all species considering scheme 1 were in the same range as that obtained experimentally (figure 5).

Comparing the voltammogram of tnz with $[Cu_2(OAc)_4(tnz)_2]$, we found a two-fold increase in reduction peak current (I_{pc}) for complex (358 μA) as compared to tnz (170 μA) (figure 3). Since equal concentrations of tnz and $[Cu_2(OAc)_4(tnz)_2]$ were used to study the electrochemical behavior, this doubling of peak current for the complex indicated the presence of two tnz units in the complex, suggesting their $-NO_2$ groups underwent reduction simultaneously.

3.5. *Interaction of tnz and $[Cu_2(OAc)_4(tnz)_2]$ with calf thymus DNA: determination of binding parameters*

The interaction of tnz and $[Cu_2(OAc)_4(tnz)_2]$ with ct DNA was studied with the help of cyclic voltammetry in aqueous solution (buffer, pH ~7.4) containing 120 mM NaCl, 3.5 mM KCl, 1 mM $CaCl_2$, and 0.5 mM $MgCl_2$ to maintain the physiological conditions. Under the experimental conditions, tnz shows a reduction peak at −710 mV, while $[Cu_2(OAc)_4(tnz)_2]$ shows a peak at −857 to −865 mV. Solutions were prepared having a constant concentration of either tnz or $[Cu_2(OAc)_4(tnz)_2]$ to which different concentrations of ct DNA were added. Cyclic voltammetry of each solution was performed and the change in cathodic peak current (ΔI) at −710 mV for tnz and −857 mV for $[Cu_2(OAc)_4(tnz)_2]$ were used to construct binding isotherms. Cyclic voltammograms of tnz and $[Cu_2(OAc)_4(tnz)_2]$ in the absence and presence of different amounts of ct DNA are shown in figure 6(a) and (b), respectively.

Upon addition of ct DNA, the reduction peak current of each compound gradually decreased. Whereas for tnz, there was no shift in reduction potential during titration, for $[Cu_2(OAc)_4(tnz)_2]$, there was an initial shift by ~6–8 mV to more negative potential that was later restored to the original reduction potential of $[Cu_2(OAc)_4(tnz)_2]$ in aqueous

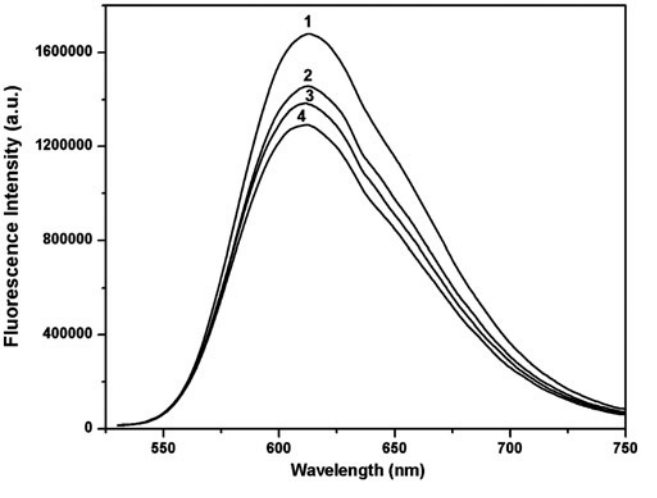

Figure 7. Variation of fluorescence intensity of a solution of ct DNA that was saturated with ethidium bromide in the absence of $[Cu_2(OAc)_4(tnz)_2]$ (1) and presence of 47.62 μM $[Cu_2(OAc)_4(tnz)_2]$ at different time intervals; 0 (2), 10 (3) and 30 min (4). pH 7.4; [NaCl] = 120 mM and [DNA] = 195 μM.

solution. Looking at the nature of the two voltammograms [figure 6(a) and (b)], as ct DNA was added the compounds interacted with it in a manner that the bound form was rendered redox inactive. For this reason, all successive reduction peak currents recorded during titration of each compound with ct DNA corresponds to that of the free compound (C_f) [28]. Studies on DNA interaction followed by cyclic voltammetry suggests if a compound gets bound to DNA and yet remains redox active with regard to the same functional group, then there should be a distinct shift in its reduction peak potential depending on the change brought about on the functional group upon binding with DNA [28, 56, 71]. On the contrary, a no shift in reduction peak potential implies, either the functional group responsible for electrochemical response was encaged or encapsulated upon binding to DNA, or that upon interaction the redox active unit present in the molecule underwent structural changes that made it electrochemically inactive [28].

In our case, since no new peak developed for both compounds during the course of titration with ct DNA, we have reason to believe that $-NO_2$ of the bound forms was not electrochemically active. For this reason, all subsequent peak currents for tnz [figure 6(a)] and $[Cu_2(OAc)_4(tnz)_2]$ [figure 6(b)] obtained upon addition of ct DNA could be assigned to

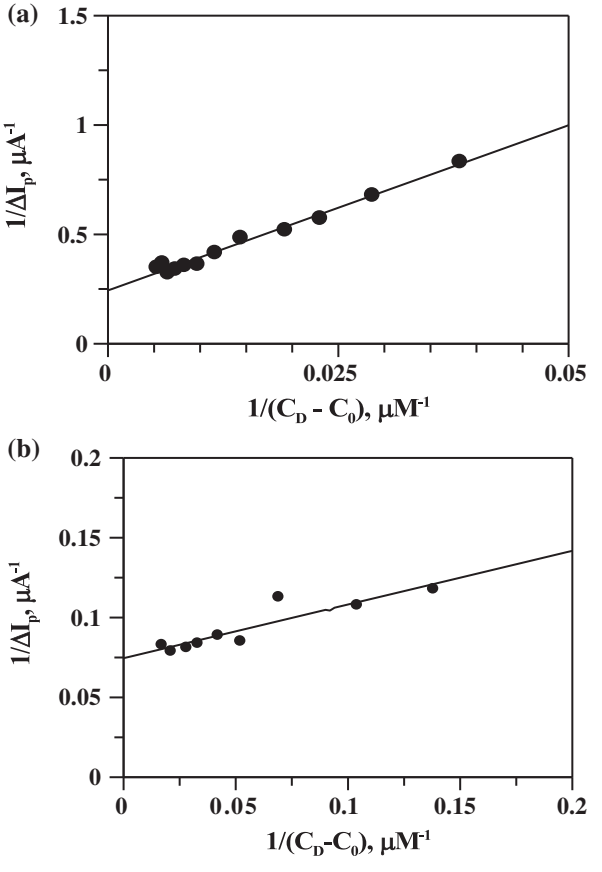

Figure 8. Double reciprocal plot for the interaction of (a) tnz and (b) $[Cu_2(OAc)_4(tnz)_2]$ with ct DNA; pH 7.4; [NaCl] = 120 mM; T = 25 °C.

Table 3. Binding constant and site size values of tnz and $[Cu_2(OAc)_4(tnz)_2]$ interacting with ct DNA.

Compounds	$K_{app} \times 10^{-4}$ (M^{-1}) from double-reciprocal plot [equation (6)]	$K_{app} \times 10^{-4}$ (M^{-1}) from nonlinear curve fitting [equation (5)]	Site size of interaction from mole ratio plot n	Overall binding constant $K^* = K_{app} \times n$ [10^{-4} (M^{-1})]	Overall binding constant $K^* \times 10^{-4}$ (M^{-1}) [equation (7)]	Site size of interaction n [equation (7)]
Tinidazole	1.60 ± 0.06	1. 57 ± 0.07	1.8 ± 0.55	3.2 ± 0.05	3.35 ± 0.39	1.40 ± 0.10
$[Cu_2(OAc)_4(tnz)_2]$	22.0 ± 3.80	24.0 ± 2.25	1.8 ± 0.60	46.0 ± 1.80	59.0 ± 6.29	1.60 ± 0.05

that of the free compound (C_f) [56]. For DNA titrations, such lack of electrochemical response of the bound form is an indication of intercalation since it leads to the molecule being locked between the strands of DNA [56]. On the contrary, other forms of binding (to DNA) keeps open the option of the bound form remaining electrochemically active.

Hence, in order to establish the mode of binding of the complex with ct DNA, experiments were performed where $[Cu_2(OAc)_4(tnz)_2]$ was allowed to interact with ct DNA that was earlier saturated with EtBr. The fluorescence maxima of the EtBr–DNA adduct obtained at 610 nm decreased considerably with increase in incubation time (figure 7), suggesting displacement of EtBr by $[Cu_2(OAc)_4(tnz)_2]$, EtBr being an established DNA intercalator, this experiment proves that $[Cu_2(OAc)_4(tnz)_2]$ must also be an intercalator.

Although mentioned in section 3.4, all electrochemical processes in aqueous solution (buffer, pH ~7.4) were purely diffusion controlled with no adsorption on the electrode surface. This was checked for DNA titration data as well by plotting I_{pc} *versus* the square root of the scan rate [71]. Results of the titrations were analyzed according to equations (4)–(7) as described under methods (section 2.2.5). From the cathodic peak current (I_{pc}) being linearly proportional to the concentration of either free tnz or free $[Cu_2(OAc)_4(tnz)_2]$ (C_f), ΔI was calculated. By plotting $1/\Delta I$ against $1/(C_D - C_0)$ for tnz [figure 8(a)] and $[Cu_2(OAc)_4(tnz)_2]$ [figure 8(b)], ΔI_{max}, i.e. maximum change in current for the interaction of the compounds with ct DNA, was obtained as the inverse of the intercept. The apparent binding constant (K_{app}), obtained as the reciprocal of K_d, was evaluated from the slope of the double reciprocal plots [figure 8(a) and (b)]. Apparent binding constants were $1.6 \times 10^4\ M^{-1}$ for tnz [figure 8(a)] and $2.2 \times 10^5\ M^{-1}$ for $[Cu_2(OAc)_4(tnz)_2]$ [figure 8(b)] (table 3). The data obtained from the titrations were analyzed by non-linear square fit analysis using equations (4) and (5), where $\Delta I/\Delta I_{max}$ was plotted against total DNA concentration (C_D). Figure 9(a) and (b) shows plots of the normalized increase of $\Delta I/\Delta I_{max}$ as a function of the concentration of ct DNA for tnz and $[Cu_2(OAc)_4(tnz)_2]$, respectively. K_{app} was determined from these plots as the reciprocal of K_d and the values were $1.57 \times 10^4\ M^{-1}$ and $2.4 \times 10^5\ M^{-1}$ for tnz and $[Cu_2(OAc)_4(tnz)_2]$, respectively (table 3). Values for K_{app} for both the compounds indicate excellent agreement between the methods of analysis.

Another very important parameter connected with studies on DNA interaction is the site size (n), i.e. the number of nucleotide bases linked to a molecule of the compound. While the binding constant indicates the strength of binding with DNA, site size n is indicative of the number of bases affected by a single molecule. Together, these two parameters indicate the level of distortion or modification on the DNA backbone following interaction with a compound. This is manifested in the efficacy of one drug over another in distorting the DNA structure. Site size of interaction was determined from the plot of normalized increase of $\Delta I/\Delta I_{max}$ as a function of the mole ratio of DNA to either compound. The insets of figures 9(a) and (b) are typical plots of $\Delta I/\Delta I_{max}$ *versus* mole ratio of [DNA]/[tnz] and

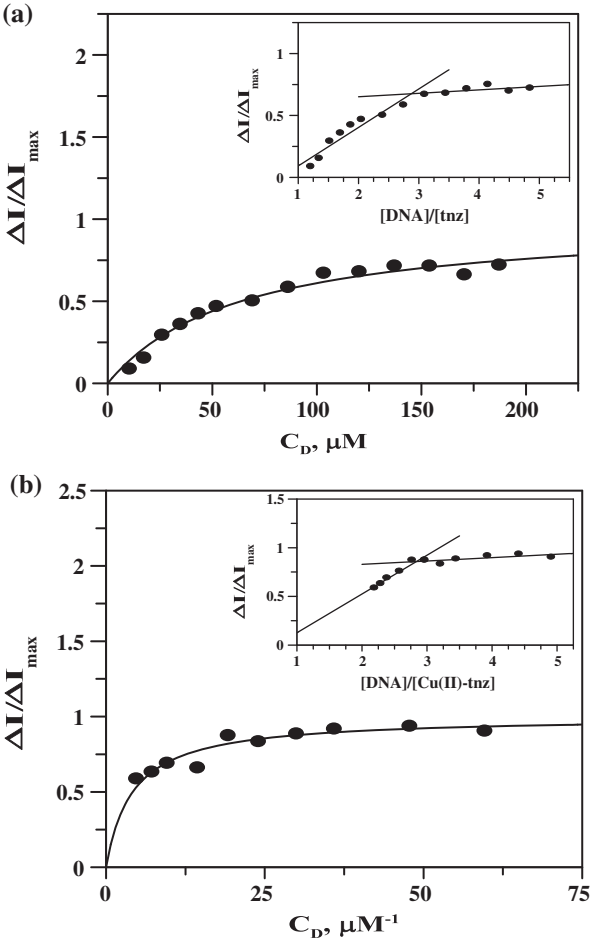

Figure 9. Binding isotherm for (a) tnz and (b) $[Cu_2(OAc)_4(tnz)_2]$ interacting with ct DNA; the line is the fitted data corresponding to a non-linear fit that follows equation (6). Inset: Plot of normalized increase of peak current as a function of mole-ratio of ct DNA to the compounds respectively; pH 7.4; [NaCl] = 120 mM; T = 25 °C.

$[DNA]/[Cu_2(OAc)_4(tnz)_2]$, respectively. In each case, the point of intersection of the two straight lines drawn using points before and after saturation gives the stoichiometry or the binding site size (n). The value of n was 1.8 (~2.0) for both compounds binding to ct DNA.

The overall binding constant for the compounds was evaluated by multiplying K_{app} with the site size n (table 3). What needs mentioning is that the overall binding constant K^* for tnz interacting with ct DNA in this study was close to that of mnz binding to ct DNA [$K = (2.2 \pm 1.3) \times 10^4\ M^{-1}$] that was evaluated by cyclic voltammetry [29].

The DNA titration results of both compounds were also fitted to equation (7) to calculate the overall binding constant (K^*) and site size of interaction (n) in yet another way [figures 10(a) and (b)]. Values obtained were $3.4 \times 10^4\ M^{-1}$ (K^*) and 1.4 (n) for tnz, while for the complex it was $5.9 \times 10^5\ M^{-1}$ (K^*) and 1.6 (n) (table 3). The results for binding parameters evaluated using equation (7) are in agreement with that determined using equations (4)–(6).

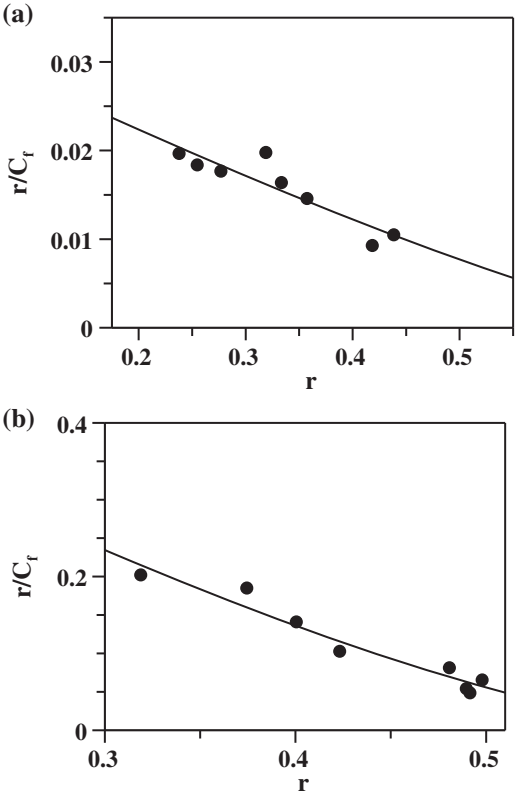

Figure 10. Voltammetric titrations of (a) tnz and (b) $[Cu_2(OAc)_4(tnz)_2]$ with ct DNA, plotted as r/C_f *vs.* r; pH 7.4; [NaCl] = 120 mM; T = 25 °C; line represents the fitted data according to equation (7).

The value obtained for $[Cu_2(OAc)_4(tnz)_2]$ was also quite close to the binding constant value of another reported Cu(II) complex having a benzimidazolyl unit [72]. The study therefore demonstrates complex formation of tnz with Cu(II) was able to cause a substantial increase in overall binding constant of tnz with ct DNA.

3.6. *Interaction of tnz and $[Cu_2(OAc)_4(tnz)_2]$ with bacterial and fungal cell lines*

Susceptibility of bacterial and fungal cells to tnz and $[Cu_2(OAc)_4(tnz)_2]$ was checked by performing MIC assay as described under methods (section 2.2.6) and presented in table S1. Control experiments were also done taking free Cu(II) as copper(II) nitrate, copper(II) acetate, a non-toxic ligand EDTA in the form of Na_2EDTA, and a complex of EDTA with Cu(II). Data reveal that $[Cu_2(OAc)_4(tnz)_2]$ was more effective than tnz against bacterial cells showing lower MIC compared to tnz. In case of the fungal cells, efficacy of tnz and $[Cu_2(OAc)_4(tnz)_2]$ was the same and showed similar MIC values. However, MIC of tnz was lower in case of *C. albicans*, the fungal cell as compared to the two bacterial cells. While the complex could improve the action of tnz toward bacterial cells, the same was not observed for the fungal cell (table S1). This suggests that complex formation of Cu(II) with tnz enabled tnz to target and kill bacterial cells more effectively than when present alone,

while the same was not true for fungal cells. Control experiments clearly showed that free Cu(II) was not active against the three types of cells with very high MIC. Experiments carried out with a Cu(II) complex of a non-toxic ligand (EDTA), i.e. Cu(II)-EDTA did not show any significant activity and results were similar to that of EDTA. Therefore, association of Cu(II) with tnz was unique in carrying out antibacterial and/or antifungal activity.

4. Conclusion

A binuclear paddle-wheel complex of Cu(II) with tnz was prepared where each tnz was linked to one Cu(II), while the Cu(II) ions were connected by four acetate bridges. The complex was characterized by single-crystal X-ray diffraction, IR, mass, EPR, elemental analysis, and cyclic voltammetry. Interaction of tnz and $[Cu_2(OAc)_4(tnz)_2]$ with ct DNA was followed by cyclic voltammetry to check whether complex formation increased DNA interaction. Results were analyzed by three different methods, leading to the determination of binding parameters. Values obtained from all three were in agreement and indicate that $[Cu_2(OAc)_4(tnz)_2]$ bound ct DNA an order of magnitude higher than tnz. The study on DNA interaction suggests $[Cu_2(OAc)_4(tnz)_2]$ could have improved action on a biological target that could help to maintain the efficacy of tnz even if generation of a nitro radical anion is reduced following complex formation. In order to verify this, compounds were treated with two bacterial cells *S. aureus* and *E. coli* and a fungal cell *C. albicans*. The findings suggest performance of $[Cu_2(OAc)_4(tnz)_2]$ on two bacterial cells was better than tnz, while in case of the fungal cell both had similar effects. Hence, coordination of Cu(II) to tnz brings about a change in its electronic environment that influenced the biological function on bacterial cells, with improved activity.

Abbreviations

tnz	tinidazole
$[Cu_2(OAc)_4(tnz)_2]$	Cu(II) complex of tinidazole
ct DNA	calf thymus DNA
MIC	minimum inhibitory concentration

Supplemental material

The CIF can be obtained free of charge at www.ccdc.cam.ac.uk/conts/retrieving.html (or from the Cambridge Crystallographic Data Center, 12 Union Road, Cambridge CB2 1EZ, UK; Fax: +44 1223 336033; E-mail: deposit@ccdc.cam.ac.uk) mentioning CCDC No. 845775.

Acknowledgements

Saurabh Das is grateful to the DST-FIST program of the Department of Chemistry, Jadavpur University, for the X-ray diffractometer facility. The authors are grateful to Dr Debojyoti Ghoshal, Department of Chemistry, Jadavpur University, for his help in analyzing the X-ray diffraction data. Saurabh Das is grateful to Prof. Amitava De of Chemical Sciences Division, Saha Institute of Nuclear Physics, Kolkata, for cyclic voltammetry experiments and Prof. Samita Basu (HOD, CSD, SINP) for fluorescence experiments. Saurabh Das is also grateful to Prof. Kalyan K. Mukherjea and his student Shiv Shankar Paul for their help in recording EPR spectra at the departmental facility. Ramesh Chandra Santra expresses his gratitude to the UGC, New Delhi, for a JRF. Piyal Das is grateful to UGC, New Delhi, for a Research Fellowship in the scheme "Scholarship for Meritorious Students".

References

[1] R.J.P. Williams. *Pure Appl. Chem.*, **54**, 1889 (1982).
[2] E.C. Theil, K.N. Raymond. In *Bioinorganic Chemistry*, I. Bertini, H.B. Gray, S.J. Lippard, J.S. Valentine (Eds), pp. 1–37, University Science Books, Mill Valley, CA (1994).
[3] F. Wang, A. Habtemariam, E.P.L. Van der Geer, R. Fernandez, M. Melchart, R.J. Deeth, R. Aird, S. Guichard, F.P.A. Fabbiani, P. Lozano-Casal, I.D.H. Oswald, D.I. Jodrell, S. Parsons, P.J. Sadler. *Proc. Natl. Acad. Sci.*, **102**, 18269 (2005).
[4] A. Majumdar, K. Pal, S. Sarkar. *Dalton Trans.*, 1927 (2009).
[5] G.E. Adams, I.R. Flockhart, C.E. Smithen, I.J. Stratford, P. Wardman, M.E. Watts. *Radiat. Res.*, **67**, 9 (1976).
[6] R.P. Mason. In *Free Radicals in Biology*, W.A. Pryor (Ed.), Vol. **V**, pp. 161–222, Academic Press, New York, NY (1982).
[7] S.N.J. Moreno, R. Docampo. *Environ. Health Perspect.*, **64**, 199 (1985).
[8] D.I. Edwards. *Biochem. Pharmacol.*, **35**, 53 (1986).
[9] J.H. Tocher, D.I. Edwards. *Free Radical Res. Commun.*, **6**, 39 (1989).
[10] D.I. Edwards. In *Comprehensive Medicinal Chemistry*, C. Hansch, P.G. Sammes, J.B. Taylor (Eds), Vol. 2, 5th Edn, pp. 725–751, Pergamon Press, Oxford (1990).
[11] J.A. Squella, J. Mosre, M. Blázquez, L.J. Nú≈nez-Vergara. *J. Electroanal. Chem.*, **319**, 177 (1991).
[12] L.J. Nuñez-Vergara, S. Bollo, A. Alvarez, J.A. Squella, M. Blazquez. *J. Electroanal. Chem.*, **345**, 121 (1993).
[13] P.C. Mandal. *J. Electroanal. Chem.*, **570**, 55 (2004).
[14] F.J.C. Roe. *J. Antimicrob. Chemother.*, **3**, 205 (1977).
[15] A.M.M. Jokipii, V.V. Myllylä, E. Hokkanen, L. Jokipii. *J. Antimicrob. Chemother.*, **3**, 239 (1977).
[16] D.I. Edwards. *Br. J. Vener. Dis.*, **56**, 285 (1980).
[17] J.G. Bartlett. *Clin. Infect. Dis.*, **18**, S265 (1994).
[18] C.K. Horlen, C.F. Seifert, C.S. Malouf. *Ann. Pharmacother.*, **34**, 1273 (2000).
[19] E.J. Olson, S.C. Morales, A.S. McVey, D.W. Hayden. *Vet. Pathol.*, **42**, 665 (2005).
[20] V. Reinhardt. *J. Med. Primatol.*, **22**, 280 (1993).
[21] J.S. Bakshi, J.M. Ghiara, A.S. Nanivadekar. *Drugs*, **15**, 33 (1978).
[22] T.B. Gardner, D.R. Hill. *Clin. Microbiol. Rev.*, **14**, 114 (2001).
[23] J.R. Schwebke, R.A. Desmond. *Am. J. Obstet. Gynecol.*, **204**, 211.e1 (2011).
[24] G.E. Kelly, W.D. Meikle, D.E. Moore. *Photochem. Photobiol.*, **49**, 59 (1989).
[25] G.P. Jacobs, N. Sade. *Int. J. Radiat. Oncol.*, **10**, 1217 (1984).
[26] J.C. Thijs, A.A. Van Zwet, W. Moolenaar, J.A.J. Oom, H. Korte, E.A. Runhaar. *Aliment Pharmacol Ther.*, **8**, 131 (2007).
[27] D. Leitsch, S. Schlosser, A. Burgess, M. Duchêne. *Int. J. Parasitol; Drugs Drug Resist.*, **2**, 166 (2012).
[28] M. Sirajuddin, S. Ali, A. Badshah. *J. Photochem. Photobiol. B: Biology*, **124**, 1 (2013).
[29] X. Jiang, X. Lin. *Bioelectrochemistry*, **68**, 206 (2006).
[30] H.B. Fung, T. Doan. *Clin. Ther.*, **27**, 1859 (2005).
[31] X.-L. Wang, M. Jiang, Y.-T. Li, Z.-Y. Wu, C.-W. Yan. *J. Coord. Chem.*, **66**, 1985 (2013).
[32] Y. Mei, J.-J. Zhou, H. Zhou, Z.-Q. Pan. *J. Coord. Chem.*, **65**, 643 (2012).
[33] S.-H. Cui, M. Jiang, Y.-T. Li, Z.-Y. Wu, X.-W. Li. *J. Coord. Chem.*, **64**, 4209 (2011).
[34] F.-M. Nie, Y. Hou, G.-N. Li. *J. Coord. Chem.*, **64**, 1042 (2011).
[35] A. Kohli, N.F.N. Smriti, K. Mukhopadhyay, A. Rattan, R. Prasad. *Antimicrob. Agents Chemother.*, **46**, 1046 (2002).
[36] K. Mukhopadhyay, T. Prasad, P. Saini, T.J. Pucadyil, A. Chattopadhyay, R. Prasad. *Antimicrob. Agents Chemother.*, **48**, 1778 (2004).

[37] Madhuri, T. Shireen, S.K. Venugopal, D. Ghosh, R. Gadepalli, B. Dhawan, K. Mukhopadhyay. *Peptides*, **30**, 1627 (2009).
[38] M.S. Nothenberg, S.B. Zyngier, A.M. Giesbrecht, M.T.P. Gambardella, R.H.A. Santos, E. Kimura, R. Najjar. *J. Braz. Chem.*, **5**, 23 (1994).
[39] N. Galván-Tejada, S. Bernès, S.E. Castillo-Blum, H. Nöth, R. Vicente, N. Barba-Behrens. *J. Inorg. Biochem.*, **91**, 339 (2002).
[40] A.I. Vogel. In *A Text Book of Quantitative Inorganic Analysis*, 3rd Edn, pp. 902, ELBS & Longman, London (1961).
[41] Bruker AXS. *SMART and SAINT*, Bruker AXS Inc., Madison, WI, USA (1998).
[42] G.M. Sheldrick, *SHELXS-97, Programs for X-ray Crystals Structure Solution*, University of Gottingen, Germany (1997).
[43] G.M. Sheldrick, *SHELXL-97, Programs for X-ray Crystals Structure Refinement*, University of Gottingen, Germany (1997).
[44] A.L. Spek. *J. Appl. Crystallogr.*, **36**, 7 (2003).
[45] L.J. Farrugia. *J. Appl. Crystallogr.*, **30**, 565 (1997).
[46] L.J. Farrugia. *J. Appl. Crystallogr.*, **32**, 837 (1999).
[47] J.E.B. Randles. *Trans. Faraday Soc.*, **44**, 327 (1948).
[48] A.J. Bard, L.R. Faulkner. *Electrochemical Methods Fundamental and Applications*., John Wiley & Sons, Inc., New York, NY (2001).
[49] C. Nervi, *ESP (Electrochemical Simulations Package). (Version 2.4)*, The program is free of charge at http://lem.ch.unito.it/chemistry/esp24b.zip.
[50] T. Ossowski, P. Pipka, A. Liwo. *Electrochim. Acta*, **45**, 3581 (2000).
[51] M. Botta, M. Ravera, A. Barge, M. Bottaro, D. Osella. *Dalton Trans.*, 1628 (2003).
[52] P.S. Guin, S. Das, P.C. Mandal. *J. Phys. Org. Chem.*, **23**, 477 (2010).
[53] P. Das, P.S. Guin, P.C. Mandal, M. Paul, S. Paul, S. Das. *J. Phys. Org. Chem.*, **24**, 774 (2011).
[54] P.S. Guin, S. Das, P.C. Mandal. *J. Inorg. Biochem.*, **103**, 1702 (2009).
[55] P.S. Guin, P. Das, S. Das, P.C. Mandal. *Int. J. Electrochem.*, Article ID 183745, 10 (2012), doi:10.1155/2012/183745.
[56] H. Ju, Y. Ye, Y. Zhu. *Electrochim. Acta*, **50**, 1361 (2005).
[57] A.W. Addison, T.N. Rao, J. Reedijk, J. van Rijn, G.C. Verschoor. *J. Chem. Soc., Dalton Trans.*, 1349 (1984).
[58] J. Zhou, L. Du, Z. Li, Y. Qiao, J. Liu, M. Zhu, P. Chen, Q. Zhao. *J. Coord. Chem.*, **66**, 2166 (2013).
[59] P.M. Selvakumar, S. Nadella, J. Sahoo, E. Suresh, P.S. Subramanian. *J. Coord. Chem.*, **66**, 287 (2013).
[60] Y.-M. Li, C.-Y. Xiao, H.-R. Feng, S.-S. Guo, S.-B. Wang. *J. Coord. Chem.*, **65**, 2820 (2012).
[61] P.M. Selvakumar, E. Suresh, S. Waghmode, P.S. Subramanian. *J. Coord. Chem.*, **64**, 3495 (2011).
[62] B.N. Figgis, R.L. Martin. *J. Chem. Soc.*, 3837 (1956).
[63] J.R. Wasson, C. Shyr, C. Trapp. *Inorg. Chem.*, **7**, 469 (1968).
[64] P.M. Selvakumar, E. Suresh, P.S. Subramanian. *Inorg. Chim. Acta*, **361**, 1503 (2008).
[65] R. Cejudo, G. Alzuet, J. Borrás, M. Liu-González, F. Sanz-Ruiz. *Polyhedron*, **21**, 1057 (2002).
[66] R.W. Jotham, S.F.A. Kettle, J.A. Marks. *J. Chem. Soc., Dalton Trans.*, 428 (1972).
[67] S. Chavan, D. Srinivas, P. Ratnasamy. *J. Catal.*, **192**, 286 (2000).
[68] B. Kozlevčar, I. Leban, I. Turel, P. Šegedin, M. Petric, F. Pohleven, A.J.P. White, D.J. Williams, J. Sieler. *Polyhedron*, **18**, 755 (1999).
[69] J. Carbajo, S. Bollo, L.J. Núñez-Vergara, P.A. Navarrete, J.A. Squella. *J. Electroanal. Chem.*, **494**, 69 (2000).
[70] J.H. Tocherz, D.I. Edwards. *Free Radical Res.*, **16**, 19 (1992).
[71] M.T. Carter, M. Rodriguez, A.J. Bard. *J. Am. Chem. Soc.*, **111**, 8901 (1989).
[72] S. Dey, S. Sarkar, H. Paul, E. Zangrando, P Chattopadhyay. *Polyhedron*, **29**, 1583 (2010).